Supplemental Information

Rational regulation of the torsion angle of covalent organic frameworks for enhanced CO_2 photoreduction to ethane

Yun Ma,[a] Qian Zhang,*[a] Hao Chen,[b] Huiyong Wang,*[a] Yunjing Deng,[a] Yingying Guo,[a] Shuaiqi Gao [a] and Jianji Wang *[a]

[a]Collaborative Innovation Center of Henan Province for Green Manufacturing of Fine Chemicals, Key Laboratory of Green Chemical Media and Reactions, Ministry of Education (China), School of Chemistry and Chemical Engineering, Xinxiang, Henan 453007, P. R. China.

[b]Xi'an University of Architecture and Technology, School of Chemistry and Chemical Engineering, Xi'an 710055, P. R. China.

*Correspondence authors.
Email: qianzhang@htu.edu.cn; hywang@htu.edu.cn; jwang@htu.edu.cn.

Table of Contents:

1. Supplemental Materials and Methods

Chemicals

$MoCl_5$ (99.6%,Energy Chemical), 2,4,6-trihydroxybenzene-1,3,5-tricarbaldehyde (Tp, 97%, Yanshen Technology), p-phenylenediamine (Pa, 99%, J&K Scientific), 4,4'-biphenylenediamine (Bd, 97%, Aladdin), 4,4"-diaminoterphenyl (Ta, 98%, Leyan), acetonitrile (MeCN, 99%, Keshi), H_2O (DI), triethanolamine (TEOA, 99%, Aladdin), tris(2,2'-bipyridyl) ruthenium(II) chloride hexahydrate (98%, Macklin), 1,3,5-trimethylbenzene (98%, Aladdin), 1,4-dioxane (99.7%, Damas-beta), 1,2-dichlorobenzene (99%, J&K Scientific), 1-butanol(98%, Aladdin), N,N-dimethylacetamide (DMAC,98%, Macklin), ethanol (99%, Keshi), acetic acid (99.9%, Macklin), tetrahydrofuran (THF, 99%, Deen reagent), methanol (99%, Keshi), acetone (99.5%, Keshi), dichloromethane (99%, Keshi), Ar gas (99.99 vol%, Xinxiang Yuxin Gas Manufacturing Co., Ltd) and CO_2 gas (99.999 vol%, Xinxiang Yuxin Gas Manufacturing Co., Ltd) were used as received.

The synthesis of COFs

Synthesis of TpPa-COF

Tp (32.5 mg, 0.15 mmol), Pa (24.6 mg, 0.225 mmol), 1,2-dichlorobenzene (1.5 mL), ethanol (1.5 mL) and 6 M aqueous acetic acid (0.4 mL) were mixed and sonicated for 10 min in a 10 mL Pyrex tube. Then, the Pyrex tube was degassed through three freeze-pump-thaw cycles and heated at 130 °C for four days. The red TpPa-COF was collected by centrifugation and washed with methanol, acetone and dichloromethane for further purification. Finally, TpPa-COF was dried in a vacuum oven at 80 °C for12 h, and the product was collected with a yield of 80%.

Synthesis of TpBd-COF

Tp (32.5 mg, 0.15 mmol), Bd (42.7, 0.225mmol), 1,2-dichlorobenzene (0.75 mL), DMAC (2.25 mL) and 6 M aqueous acetic acid (0.3 mL) were mixed and sonicated for 10 min in a 10 mL Pyrex tube. Then, the Pyrex tube was degassed through three freeze-pump-thaw cycles and

then heated at 120 °C for three days. The brown TpBd-COF was collected by centrifugation and washed with DMAC, DMF, H_2O, acetone and THF for further purification. Finally, the TpBd-COF was dried in a vacuum oven at 80 °C for 12 h, and the product was collected with a yield of 80%.

Synthesis of TpTa-COF

Tp (11 mg, 0.05 mmol), Ta (0.075 mmol), 1,4-dioxane (0.6 mL), mesitylene (0.6 mL) and 6 M aqueous acetic acid (0.2 mL) were mixed and sonicated for 10 min in a 10 mL Pyrex tube. Then, the Pyrex tube was degassed through three freeze-pump-thaw cycles and then heated at 120 °C for three days. The brown TpTa-COF was collected by centrifugation and washed with acetone and THF for further purification. Finally, the TpTa-COF was dried in a vacuum oven at 80 °C for12 h, and the product was collected with a yield of 70%.

Synthesis of Tp-COFs-Mo

Tp-COFs (10 mg), $MoCl_5$ (20 mg), and 2,2'-bipyridine (23 mg) were added into a round-bottom flask containing 20 mL acetonitrile. Then, the mixture was sonicated until uniformly dispersed in the flask, which was then refluxed at 95 °C for 24 h under an argon atmosphere. After centrifuge, the resultant powder was washed several times with acetonitrile. Finally, the product was dried at 80 °C under vacuum for 12 h.

Materials characterizations

Fourier transform infrared (FT-IR) spectrometer (PerkinElmer, jx20112184) was used to determine the chemical structure of COFs powders within a wavelength range of 4000-800 cm^{-1}. X-ray diffraction (XRD) patterns of all powder samples were measured by a X'Pert3 Powder Advance diffractometer (PANalytical B.V.) with monochromatized Cu Kα radiation operating at 45 kV and 40 mA. The morphology of the materials was analyzed using a field emission scanning electron microscope (SEM) (Hitachi High-Tech Corporation, Lambd 950). X-ray photoelectron spectroscopy (XPS) and quasi-in-situ XPS spectra were recorded using a Thermo Scientific K-Alpha electron energy spectrometer (ESCALAB250Xi) with Al Kα (1486.6 eV) radiation as the X-ray excitation source and all XPS data were corrected by standard C 1s peak

(284.6 eV). Transmission electron microscope (TEM) images and energy-dispersive X-ray spectra (EDS) were acquired using a JEM-ARM300F electron microscope (JEOL Ltd) at 200 kV. The N_2 adsorption-desorption isotherms of COFs at 77 K were measured using an IQ physical adsorption instrument (Quantachrome Instruments, Autosorb IQ Station). The specific surface area and pore size distribution of the materials were analyzed using the Brunauer-Emmett-Teller (BET) and Nonlocal Density Function Theory (NLDFT) methods, respectively. The absorption range and band gap width of different COFs were determined by solid-state ultraviolet-visible diffuse reflectance spectroscopy (UV-vis DRS) (PerkinElmer, Spectrumlab 752s). The thermal stability of COFs was tested using a comprehensive thermal analyzer (TGA) (NETZSCH, STA449C) under a N_2 atmosphere, with a heating rate of 10℃ min^{-1} and a temperature range from room temperature to 800℃. The inductively coupled plasma-mass spectrum (ICP-MS) of metal elements was recorded on the Agilent 7700 spectroscopy (PerkinElme, ELAN DRC-e). Electrochemical tests were performed by a CHI 660E electrochemical working station (Shanghai). The steady-state photoluminescence (PL) spectra and PL decay spectra were measured by a FLS980 Fluorescence Spectrometer (UK). X-ray absorption fine structure (XAFS) spectra (Mo K-edge) were collected at the 1W1B station in Beijing Synchrotron Radiation Facility (BSRF) operated at 2.5 GeV with a maximum current of 250 mA.

Photoelectrochemical measurements

The photoelectrochemical measurements were carried out by a Gamry CHI 660E electrochemical workstation with a standard three-electrode system. For the three-electrode system, the saturated Ag/AgCl electrode, Pt mesh (1.0×1.0 cm^2), and the photocatalysts modified indium tin oxide (ITO) glass were used as the reference electrode, counter electrode, and working electrode, respectively. For the preparation of working electrode, 5.00 mg of the as-prepared photocatalyst and 15 μL of Nafion solution were dispersed in 85 μL ethanol, and sonicated for 30 min. Then, the 100 μL photocatalyst colloid was spread evenly on the surface of ITO conductive glass (1.0×1.0 cm^2). After drying in the air at room temperature, the working

electrode was stored in petri dishes for related tests. The photoelectric test was carried out in 0.200 M aqueous sodium sulfate solution under light illumination or dark, and 300 W Xe lamp (420 nm cut-off filter) was used as a light source. Mott-Schottky (M-S) plots were determined at the frequencies of 500, 1000 and 15000 Hz, respectively, and EIS measurements were performed in the frequency range from 100 kHz to 0.01 Hz.

Photocatalytic CO_2 reduction measurements

The photocatalytic experiments were carried out according to the reported method[1]. Briefly, in a 250 mL of optical reaction vessel (PQ256, Beijing Perfect Light Technology Co., Ltd), the catalyst (2.00 mg) was dispersed in 50 mL of acetonitrile/H_2O (v:v = 49:1) mixed solution under ultrasound. Then, 5 mL of sacrificial reagent TEOA and 6.00 mg of photosensitizer $[Ru(bpy)_3]Cl_2 \cdot 6H_2O$ were dissolved in this mixture at 25 °C. Prior to light illumination, high-purity CO_2 (99.999%) gas was injected into the closed system to remove the air, and CO_2 gas was then bubbled through the reactor for 30 min to reach fully saturation of CO_2 in the solution at 1 atm. Thereafter, the system was irradiated using a Microsolar 300 W Xe lamp with 420 nm cut-off filter (light intensity was 300 mW cm^{-2}), and the temperature of the reactor was maintained at 25 °C by circulating water from a constant temperature water bath. The generated hydrocarbon fuel products were analyzed by a 9790II gas chromatography (Fuli, China) equipped with a thermal conductivity detector (TCD) and a flame ionization detector (FID). In the test of photocatalytic stability, the catalyst after initial use was washed with water and then separated by a high-speed centrifuge for the next run. After that, the recycled catalyst was dried overnight under vacuum at 80 °C. In addition, the products in the liquid phase of the reactor were detected by ^1H NMR spectroscopy (Bruker AVIII HD 600 instrument at 600 MHz). Isotope labeling measurements were performed by using $^{13}CO_2$ gas (enrichment, 99 at.%, Sigma-Aldrich Co., Ltd) as the carbon source, and the gas product was identified by gas chromatography-mass spectrometry (GC-MS, Agilent GC/MS-7000D).

In the photocatalytic CO_2 reduction reaction, electron selectivity is defined as the percentage of electrons consumed for the formation of a target product (such as C_2H_6) relative

to the total number of electrons consumed by all reduction products.[2] According to the standard reduction half-reactions, the number of transferred electrons required for the formation of C_2H_6 is 14e, C_2H_4 is 12e, and both H_2 and CO are 2e. The formula for calculating the electron selectivity of C_2H_6 is given as follows [3]:

$$S_{C_2H_6} = 14\times R_{C_2H_6} / (14\times R_{C_2H_6} + 2\times R_{CO} + 12\times R_{C_2H_4} + 2\times R_{H_2}) \times 100\% \quad (S1)$$

where R represents the production rate of each product.

Apparent quantum efficiency of C_2H_6

The apparent quantum efficiency (AQE) was measured under the same photocatalytic reaction conditions after irradiated by different wavelengths of light (including 420, 450, 520 and 550 nm) for 1 h, and the intensity of monochromatic light was measured by a light power meter (Newport 91150-2000, USA Newport Corporation). After the test, 500 μL of the gas product was pipetted for analysis. The AQE values were calculated according to the below equation[4, 5]:

$$AQE = (14\times n_{C_2H_6}\times N_A\times h\times c)\times 100\% / (S\times P\times T\times \lambda) \quad (S2)$$

where N_A is Avogadro's constant (6.022×10^{23} mol^{-1}), h is Planck's constant (6.626×10^{-34} $J\cdot s$), c is the speed of light (3×10^8 $m\cdot s^{-1}$), P is the light intensity ($W\cdot cm^{-2}$), S is the illuminated area (cm^2), T is the illumination time (s), and λ is the wavelength of monochromatic light.

In situ ATR-FTIR spectrum measurements

The in-situ ATR-FTIR measurements were performed by a Bruker VERTEX 70v (Germany) with a mercury cadmium telluride (MCT) detector in the system. First, the COF powder was evenly spread on a polished silicon column using Nafion. Then, it was placed in the dark and sealed in a chamber, and purged with Ar until no CO_2 was detected in the system. Subsequently, CO_2 was introduced at a flow rate of 100 mL min^{-1} until CO_2 adsorption reached saturation in the photocatalytic system. Finally, visible light irradiation was applied. Infrared spectra were collected every 10 minutes from the start of the irradiation until 90 minutes.

Computational Methods

All DFT calculations were performed using the plane-wave basis set approach as implemented in the Vienna ab initio simulation package (VASP)[6]. The projector augmented wave (PAW) method was used to represent the ion-core electron interactions[7]. The valence electrons were represented with a plane wave basis set with an energy cutoff of 450 eV. Electronic exchange and correlation were described with the Perdew-Burke-Ernzerhof (PBE) functional[8]. DFT-D3 method was used to treat the van der Waals interaction[9]. A 1×1×1 Monkhorst-Pack scheme was used to generate the k-point grid for the modeled structure. The convergence criteria for the self-consistent electronic structure and geometry were set to 10−5 eV and 0.03 eV/Å, respectively. Zero-point vibrational energy (ZPVE) corrections were calculated by assuming a quantum harmonic oscillator possessing the calculated vibrational frequency.

2. Supplemental Figure S1-S38

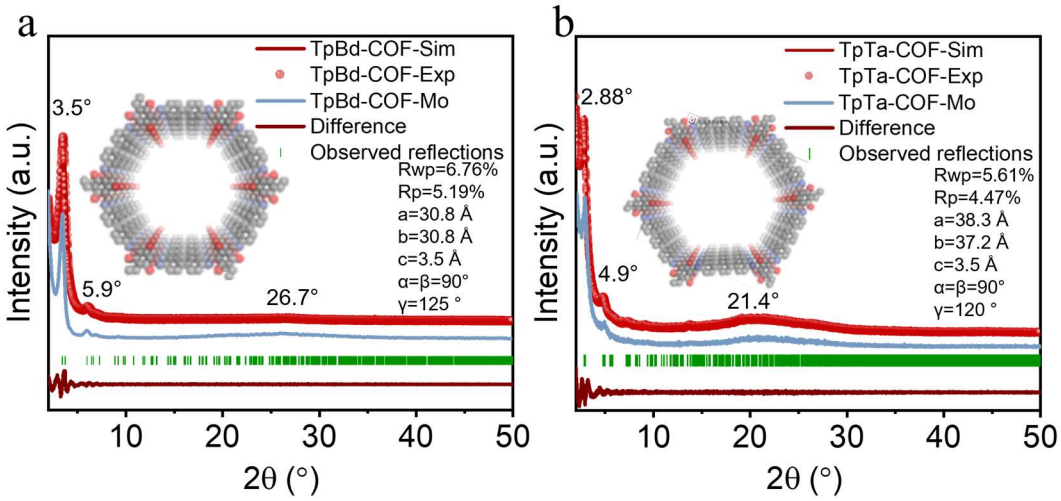

Figure S1. XRD patterns of (a) TpBd-COF-Mo, and (b) TpTa-COF-Mo.

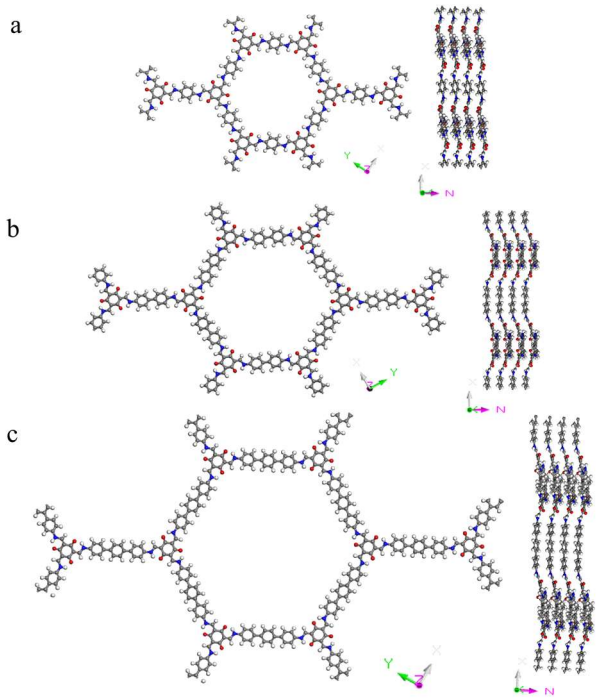

Figure S2. Optimized crystal structure models of Tp-COFs, displaying the top view (left) and corresponding side view (right) of the layered stacking configuration.

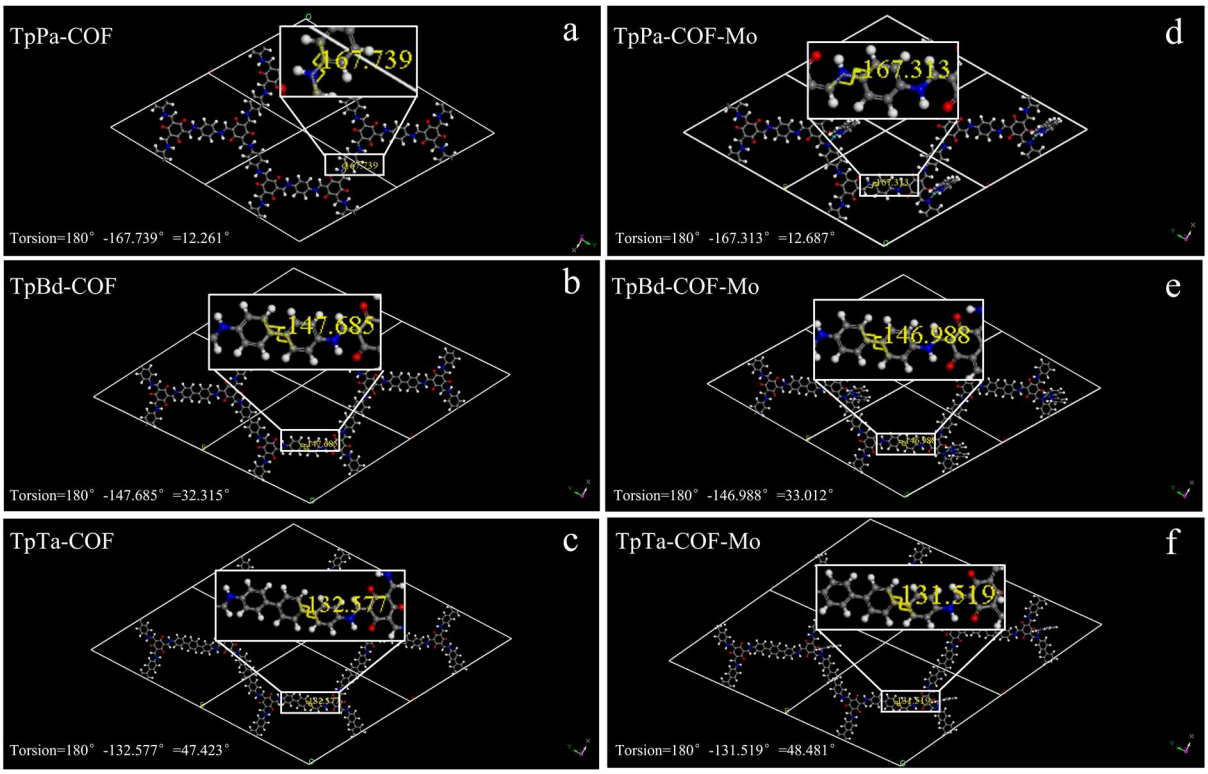

Figure S3. Torsion angles derived from the XRD data of Tp-COFs and Tp-COFs-Mo fitted by MS.

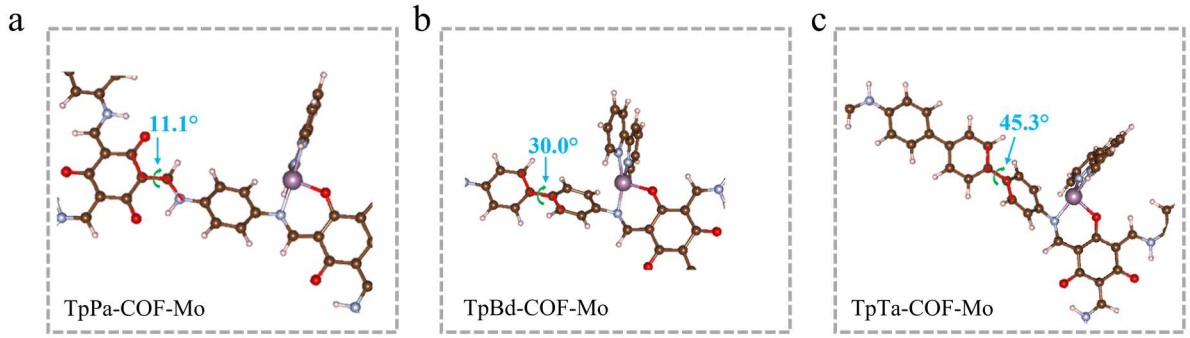

Figure S4. Torsion angles of Tp-COFs-Mo calculated by density functional theory.

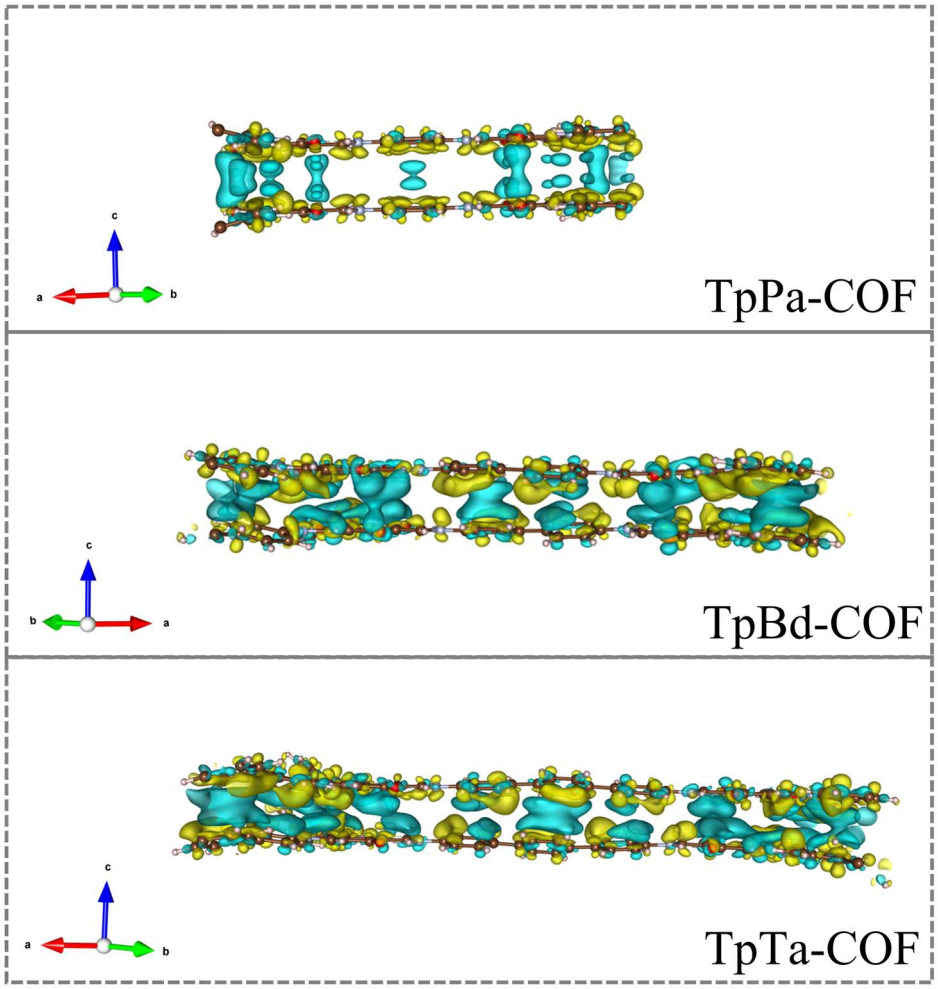

Figure S5. The charge density difference analysis via a bilayer structure of TpPa-COF, TpBd-COF and TpTa-COF, where the yellow and cyan regions represent the areas of electron accumulation and depletion, respectively. The isosurface value is set to 0.0002 eV·Å^{-3}.

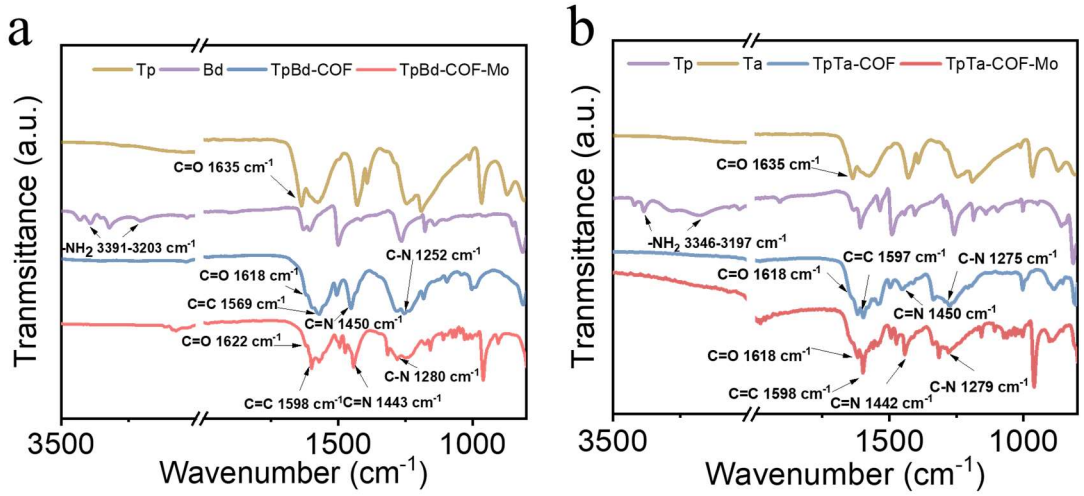

Figure S6. FTIR spectra of (a) TpBd-COF-Mo, and (b) TpTa-COF-Mo.

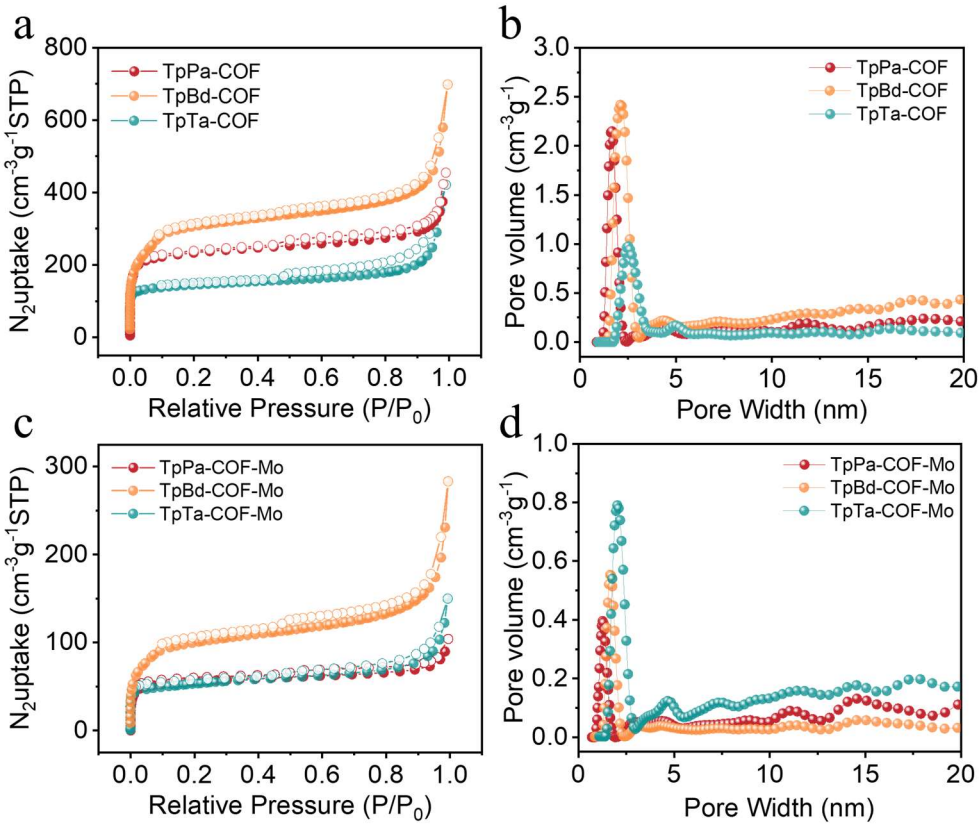

Figure S7. The calculated non-local density functional theory (NLDFT) model for Tp-COFs and COFs-Mo. (a) N_2 adsorption-desorption isotherms and (b) Pore size distribution of Tp-COFs. (c) N_2 adsorption-desorption isotherms and (d) Pore size distribution of Tp-COFs-Mo.

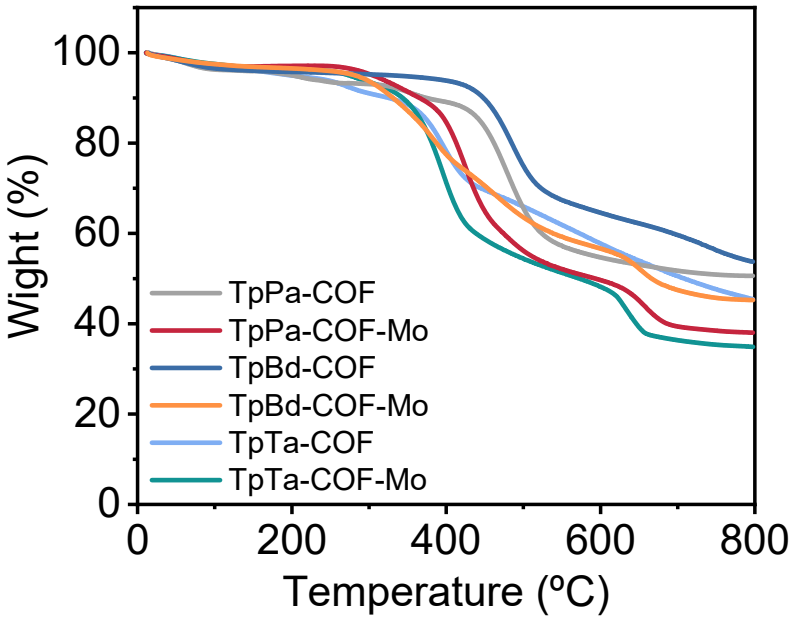

Figure S8. TGA curves of all the samples under argon gas.

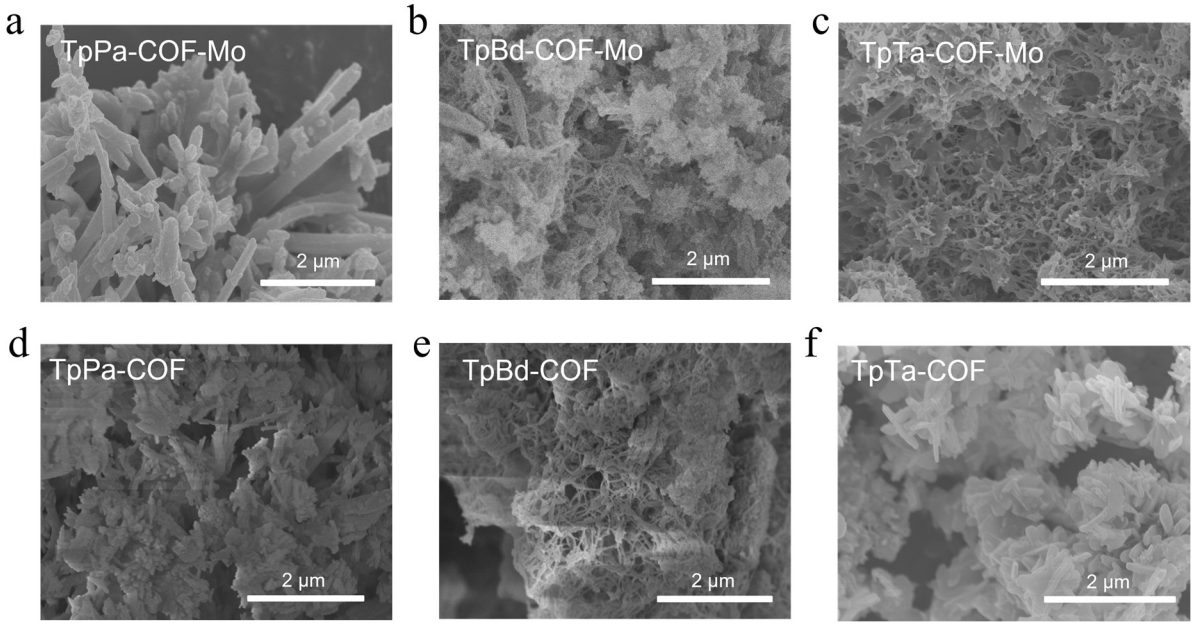

Figure S9. SEM images of (a) TpPa-COF-Mo, (b) TpBd-COF-Mo, (c) TpTa-COF-Mo, (d) TpPa-COF, (e) TpBd-COF, and (f) TpTa-COF.

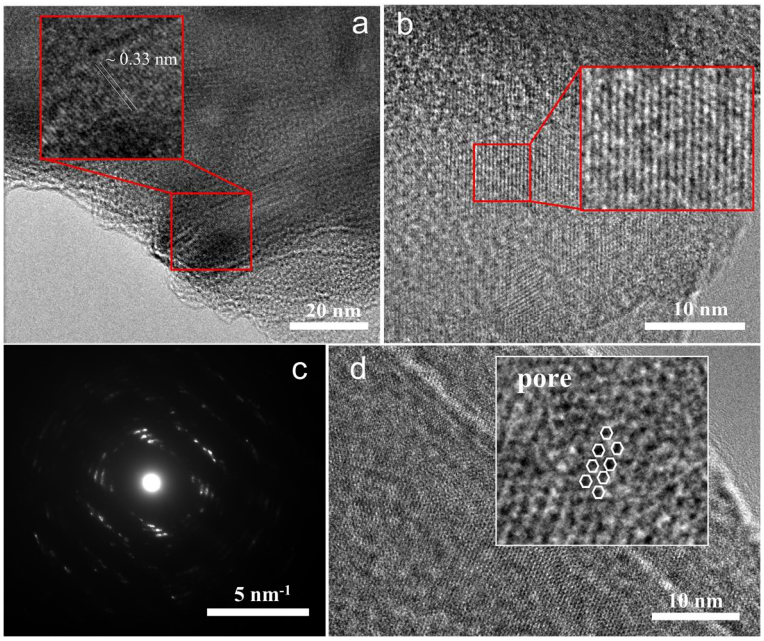

Figure S10. High-Resolution Transmission Electron Microscopy (HRTEM) images and the corresponding Selected Area Electron Diffraction (SAED) pattern for TpPa-COF-Mo.

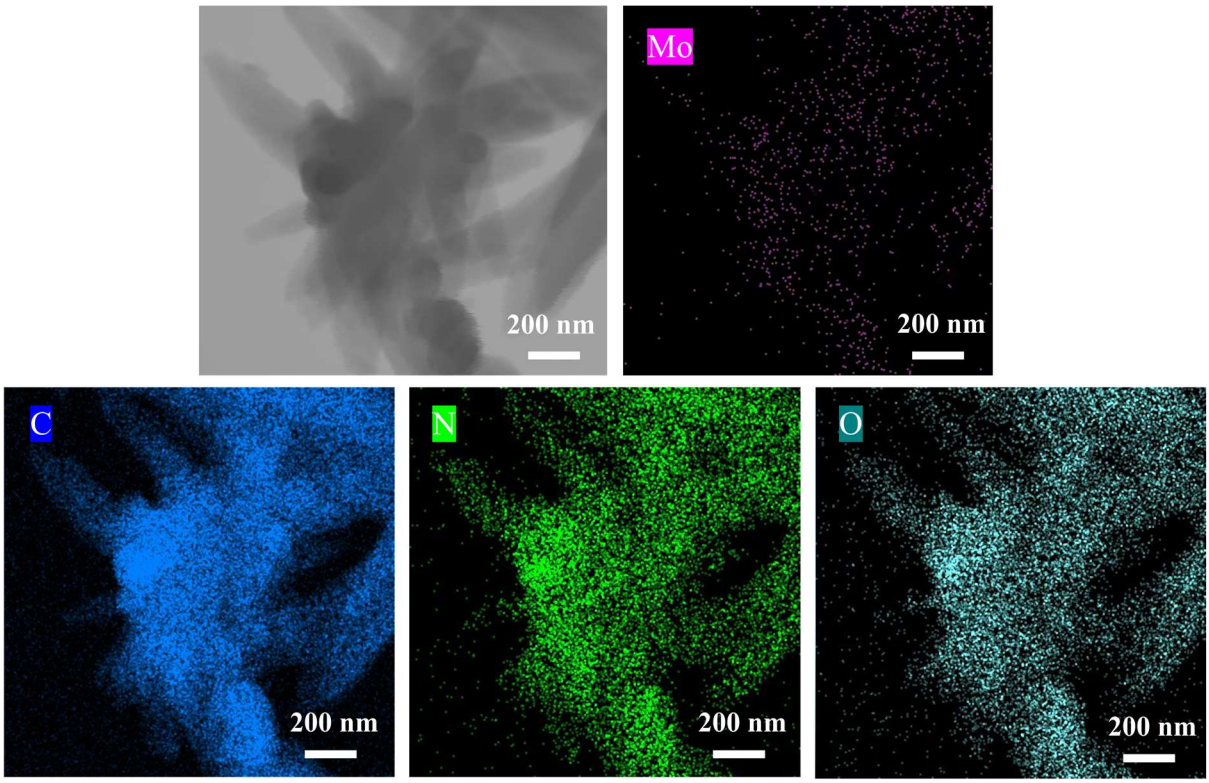

Figure S11. Energy dispersive X-ray (EDX) mappings of TpPa-COF-Mo, molybdenum mapped in purple, carbon mapped in blue, nitrogen mapped in green and oxygen mapped in cyan.

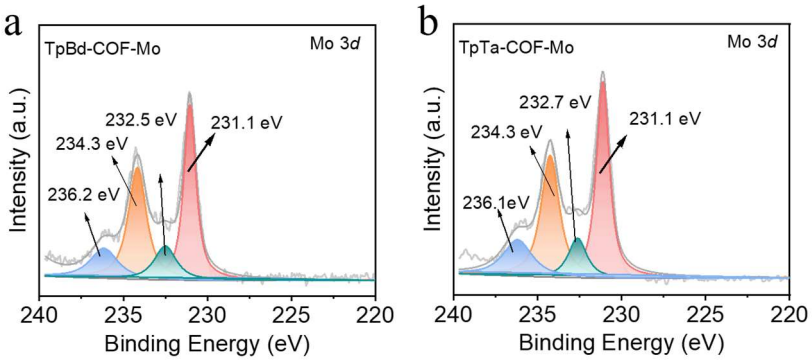

Figure S12. XPS survey spectrum of different COFs. (a) High-resolution XPS spectra of Mo 3*d* for TpBd-COF-Mo. (b) High-resolution XPS spectra of Mo 3*d* for TpTa-COF-Mo.

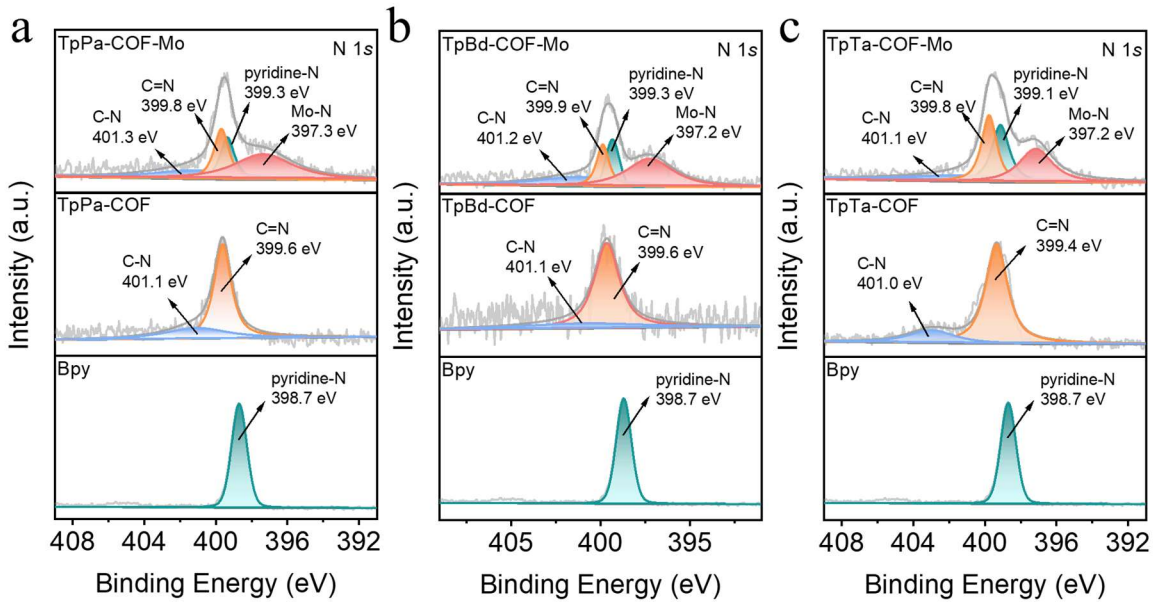

Figure S13. High-resolution XPS spectra of N 1*s* for Tp-COFs-Mo, Tp-COFs and 2,2'-bipyridine.

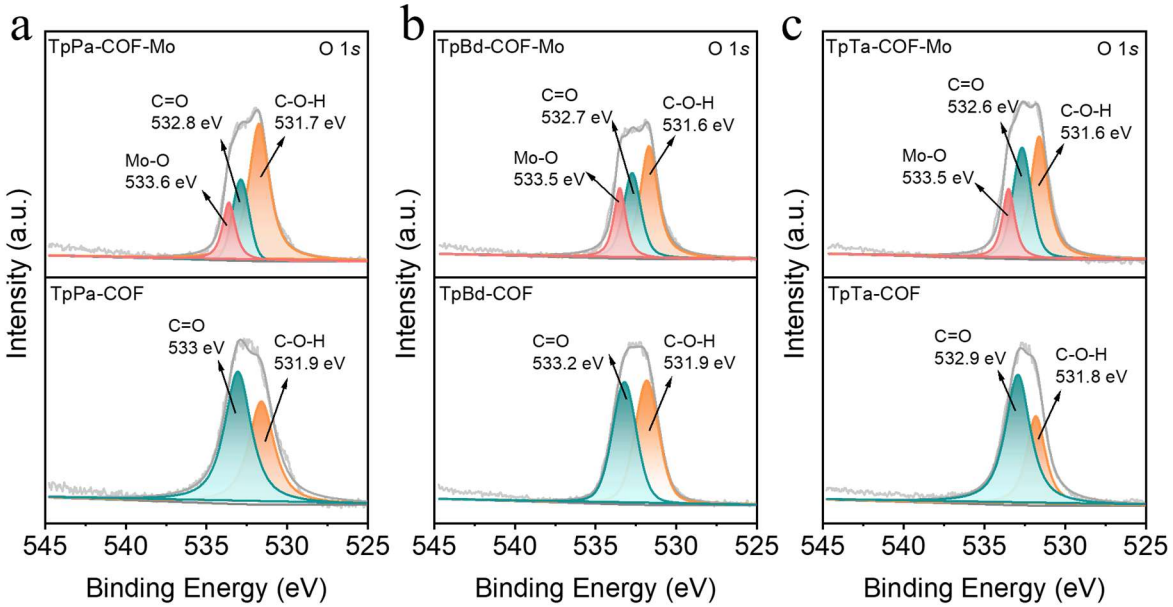

Figure S14. High-resolution XPS spectra of O 1*s* for Tp-COFs-Mo and Tp-COFs.

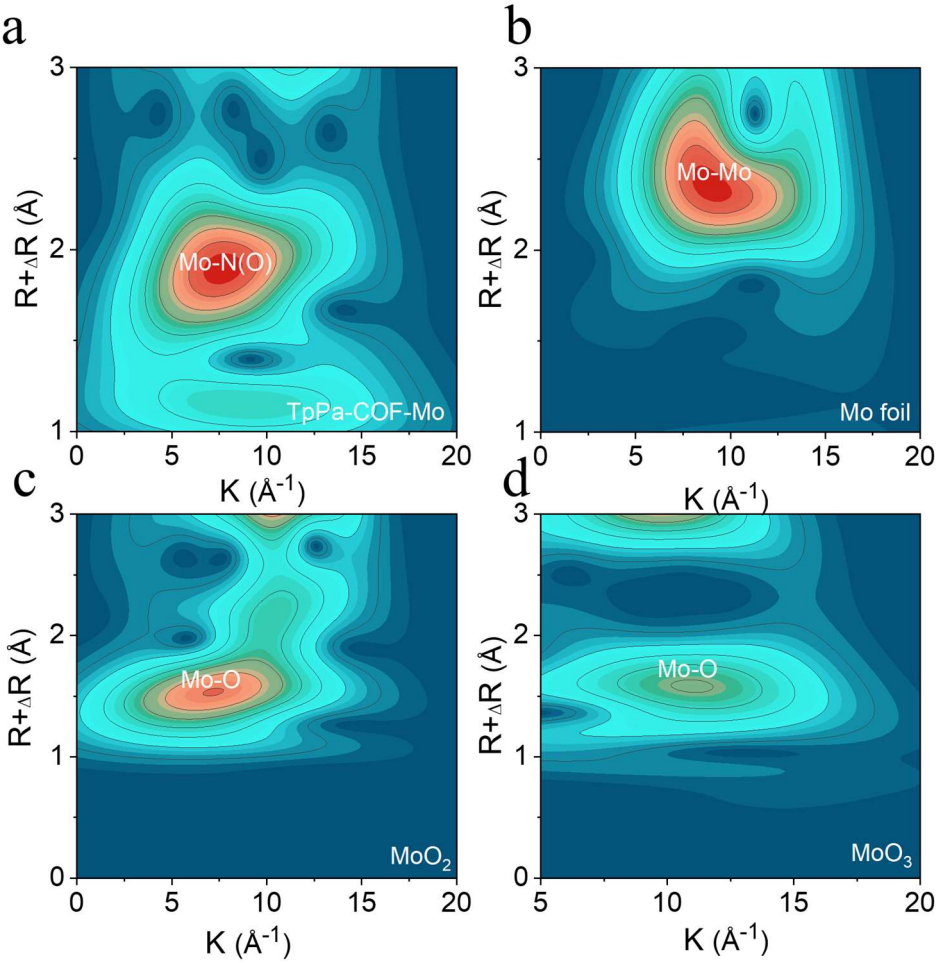

Figure S15. WT-EXAFS spectrum of discriminating radial distance and k-space resolution of TpPa-COF-Mo, Mo foil, MoO_2, and MoO_3.

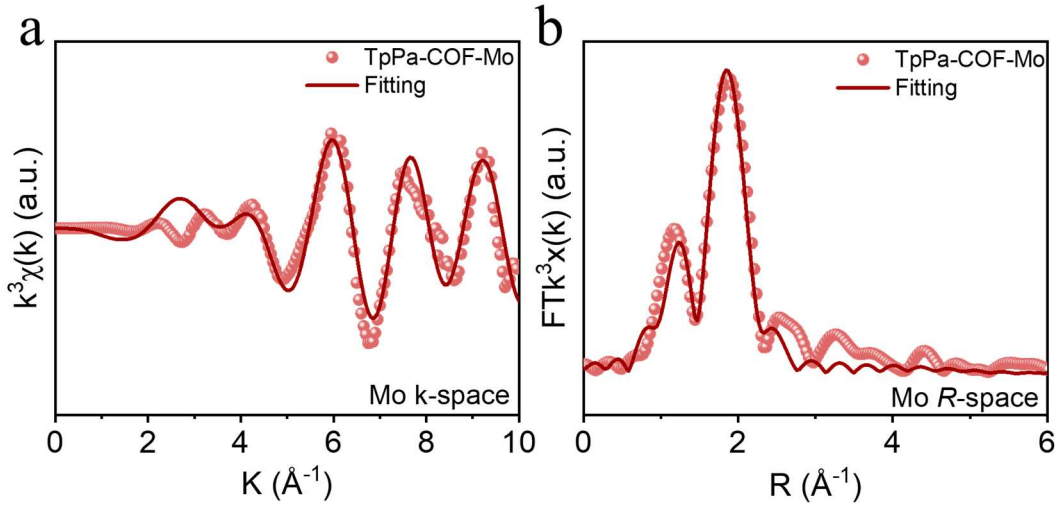

Figure S16. EXFAS fitting curves for TpPa-COF-Mo. (a) in Mo k-space and (b) in Mo R-space.

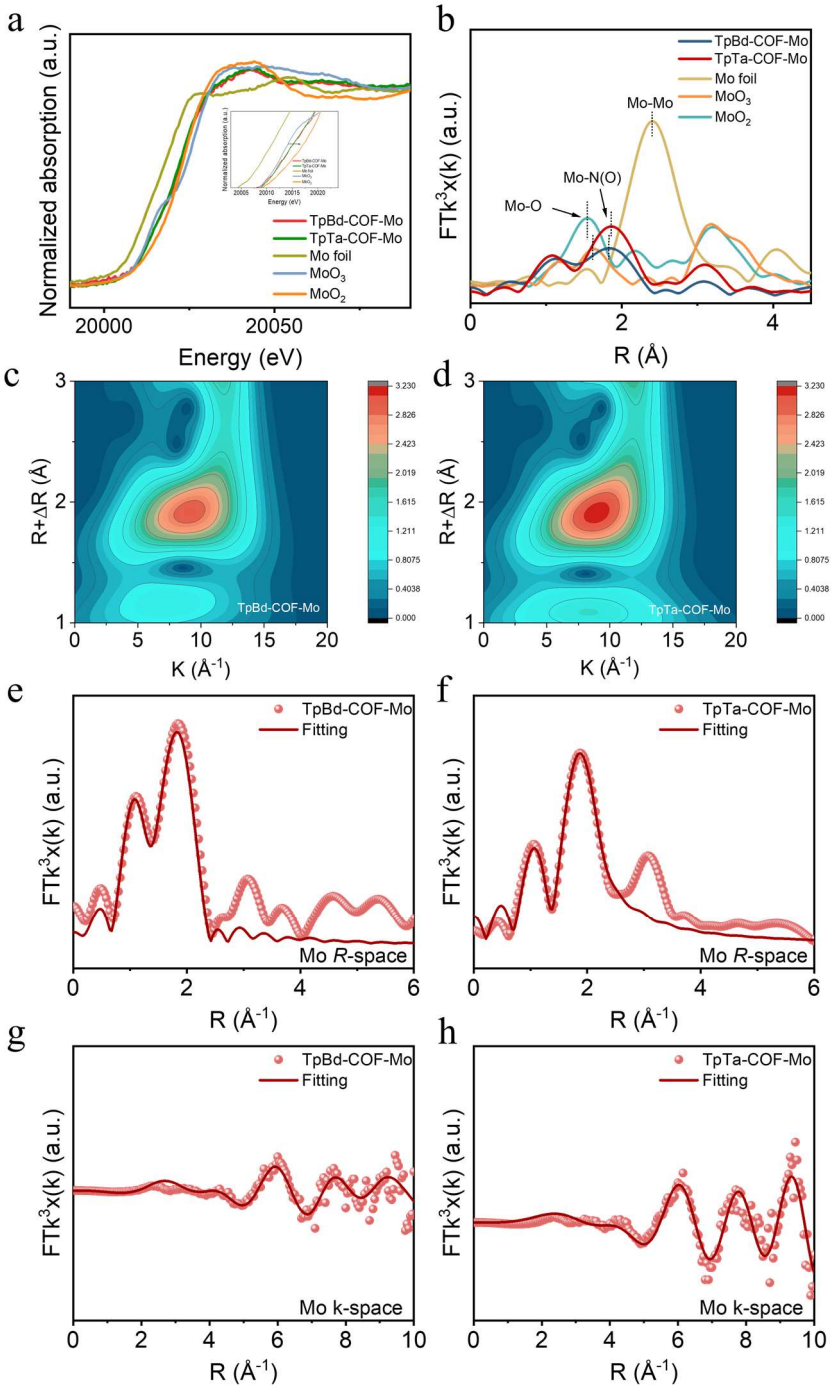

Figure S17. (a, b) Normalized XANES and FT-EXAFS spectra at the Mo k-edge of TpBd-COF-Mo, TpTa-COF-Mo, Mo foil, MoO_2, and MoO_3 samples. (c, d) WT-EXAFS spectrum of discriminating radial distance and k-space resolution of TpBd-COF-Mo and TpTa-COF-Mo. EXFAS fitting curves for TpBd-COF-Mo and TpTa-COF-Mo. (e, f) in Mo *R*-space and (g, h) in Mo k-space.

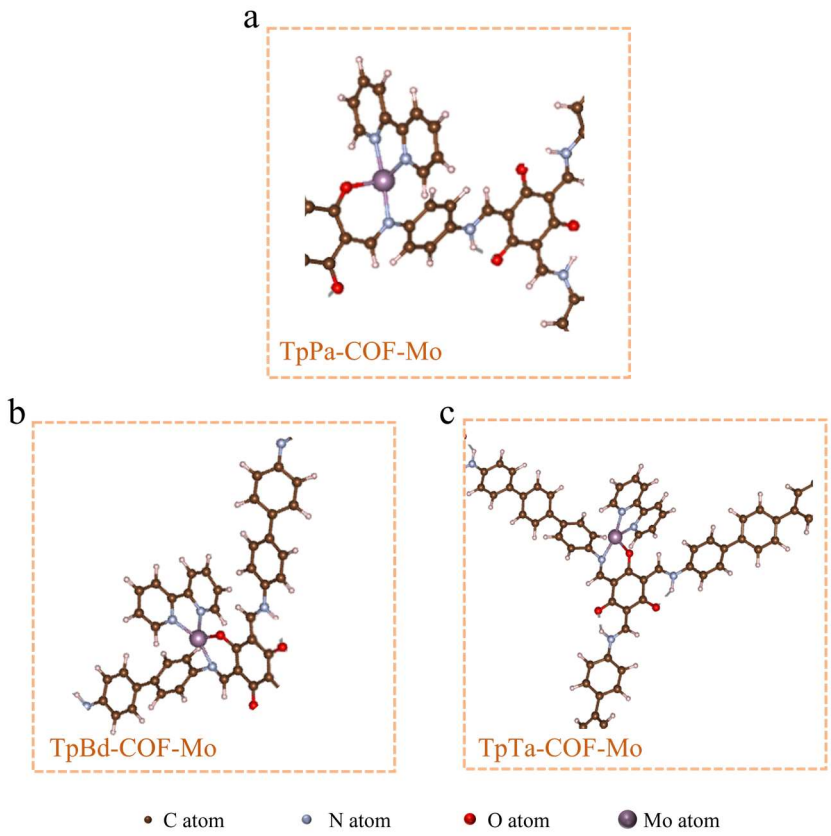

Figure S18. Simulated coordination structure of Tp-COFs-Mo fragments.

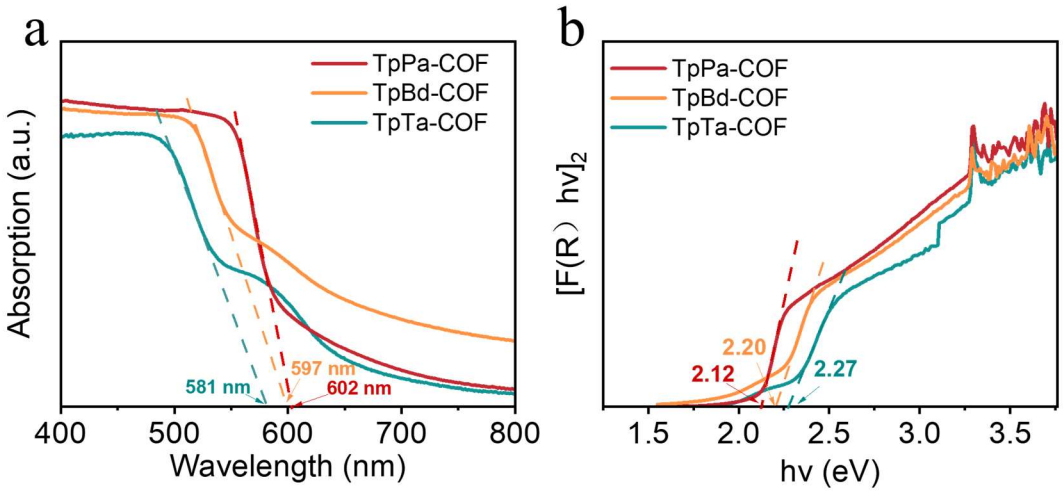

Figure S19. (a) Solid-state UV-vis diffuse reflectance spectra and (b) Tauc plots derived from solid-state UV-vis diffuse reflectance spectra of Tp-COFs.

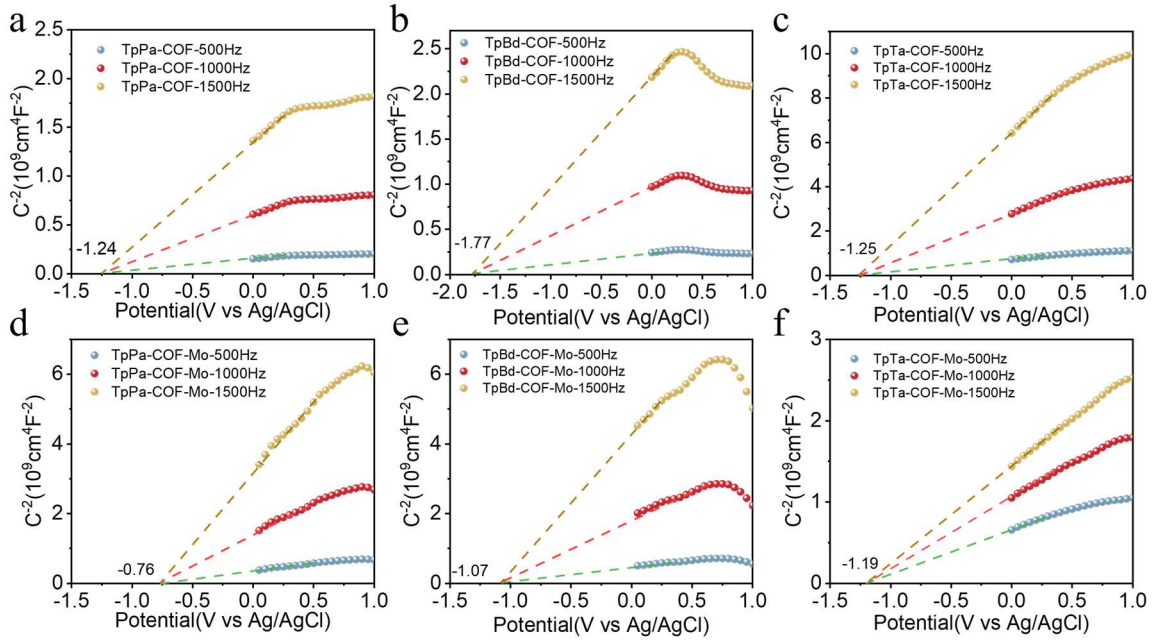

Figure S20. Mott-Schottky plots of Tp-COFs and Tp-COFs-Mo at different frequencies (500, 1000, and 1500 Hz).

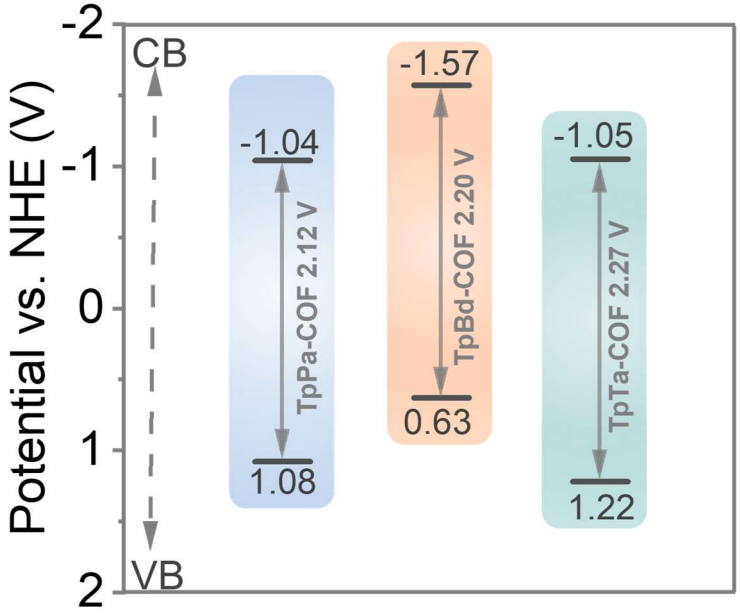

Figure S21. Band structures of Tp-COFs.

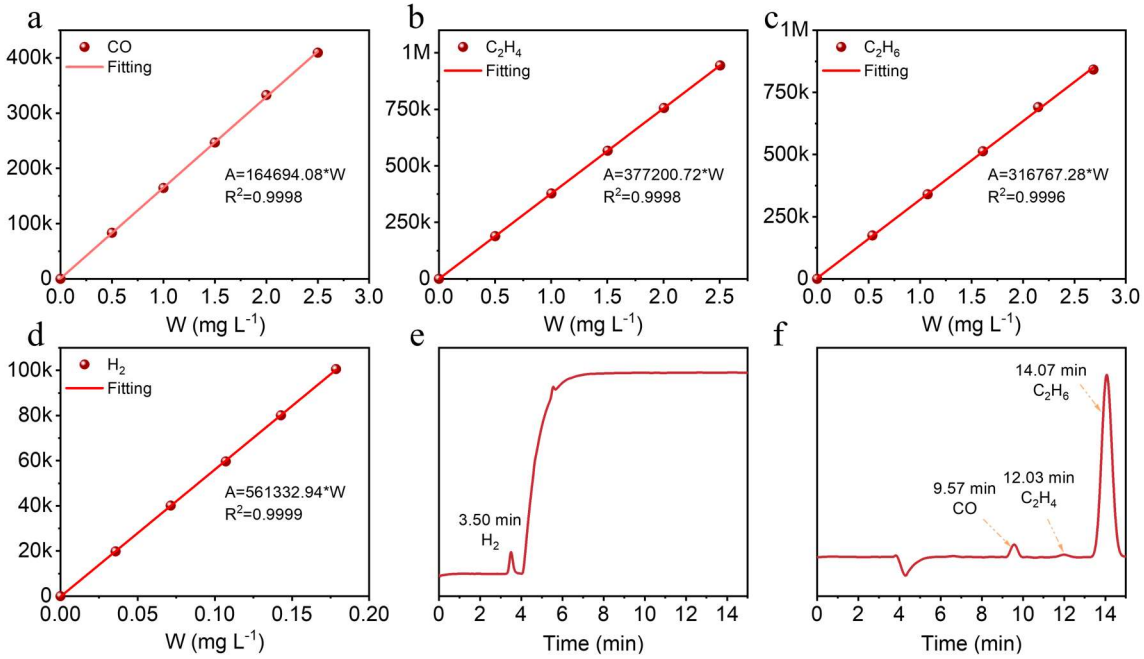

Figure S22. Linear GC calibration plots: (a) CO, (b) C_2H_4, (c) C_2H_6 and (d) H_2. The corresponding retention time based on the GC profile of the TpPa-COF-Mo: (e) H_2 and (f) CO and hydrocarbon.

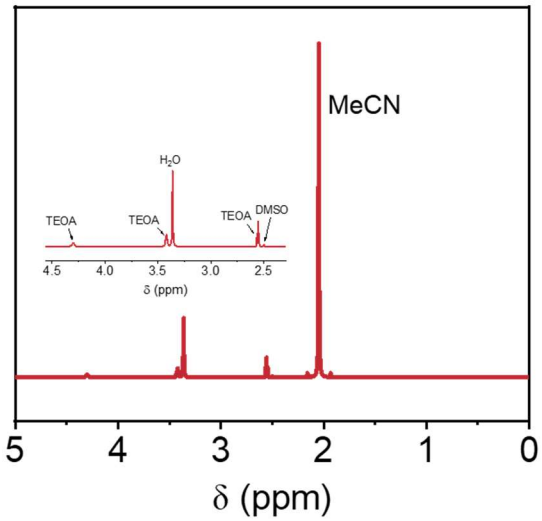

Figure S23. ^{1}H-NMR spectra of the liquid products after 2 h photoreduction. d^6-DMSO was used as the internal standard.

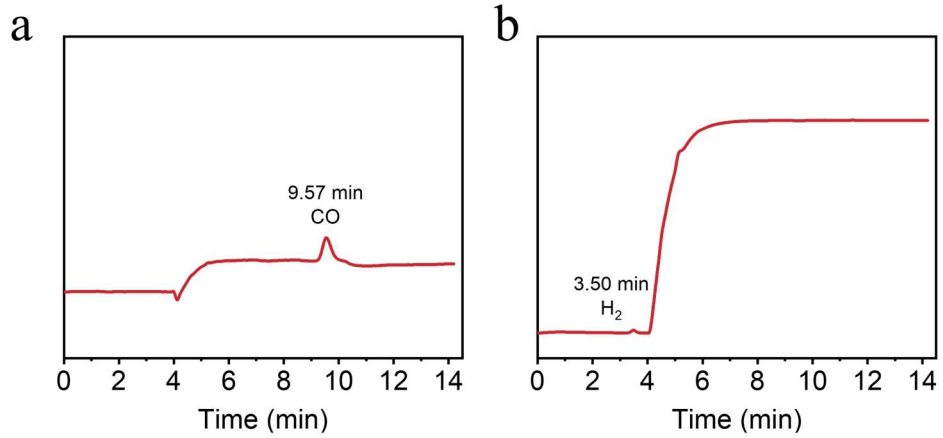

Figure S24. The corresponding retention time based on the GC profile of the TpPa-COF: (a) CO and (b) H_2.

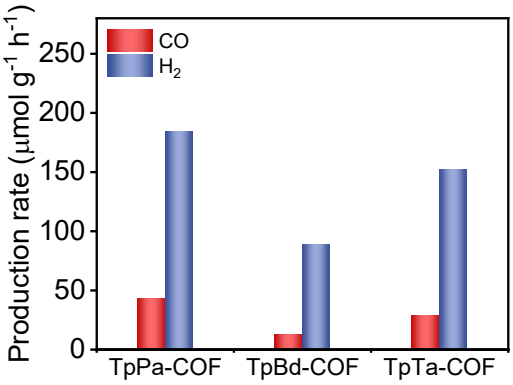

Figure S25. Comparison of the photocatalytic CO_2 reduction performance for different Tp-COFs.

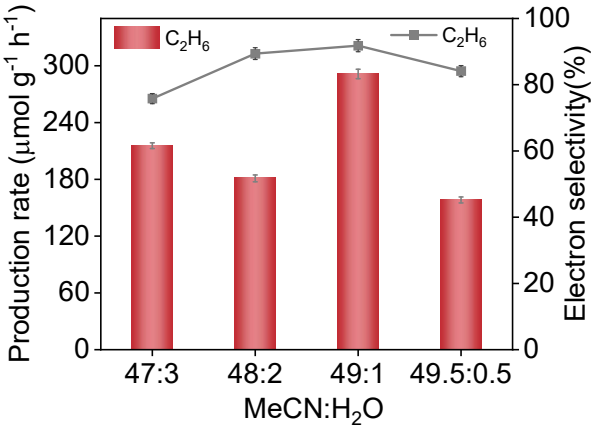

Figure S26. The evolution and electron selectivity of C_2H_6 over TpTa-COF-Mo with different volume ratios of acetonitrile/ H_2O. The error bars for C_2H_6 evolution uncertainty represent the standard deviation based on three independent measurements of each sample.

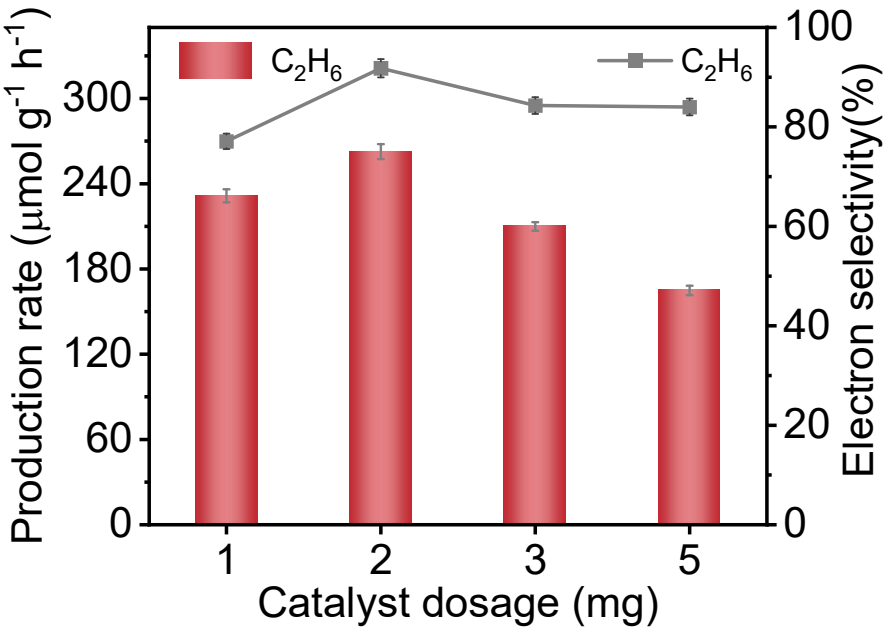

Figure S27. The effect of the catalyst dosage of the mass of the catalyst on the evolution and the electron selectivity of C_2H_6. The error bars for C_2H_6 evolution uncertainty represent the standard deviation based on three independent measurements of each sample.

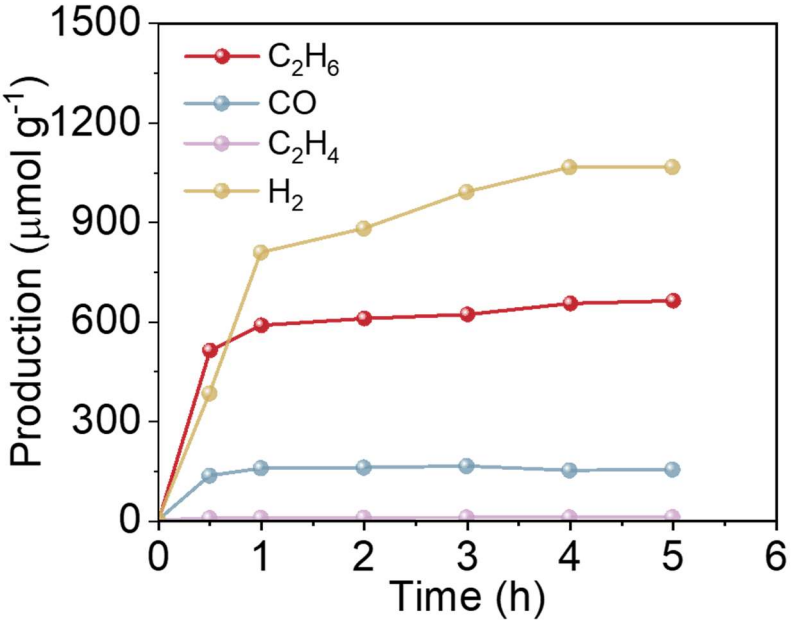

Figure S28. The production of gaseous products with irradiation time for the CO_2RR catalyzed by TpPa-COF-Mo under visible light irradiation.

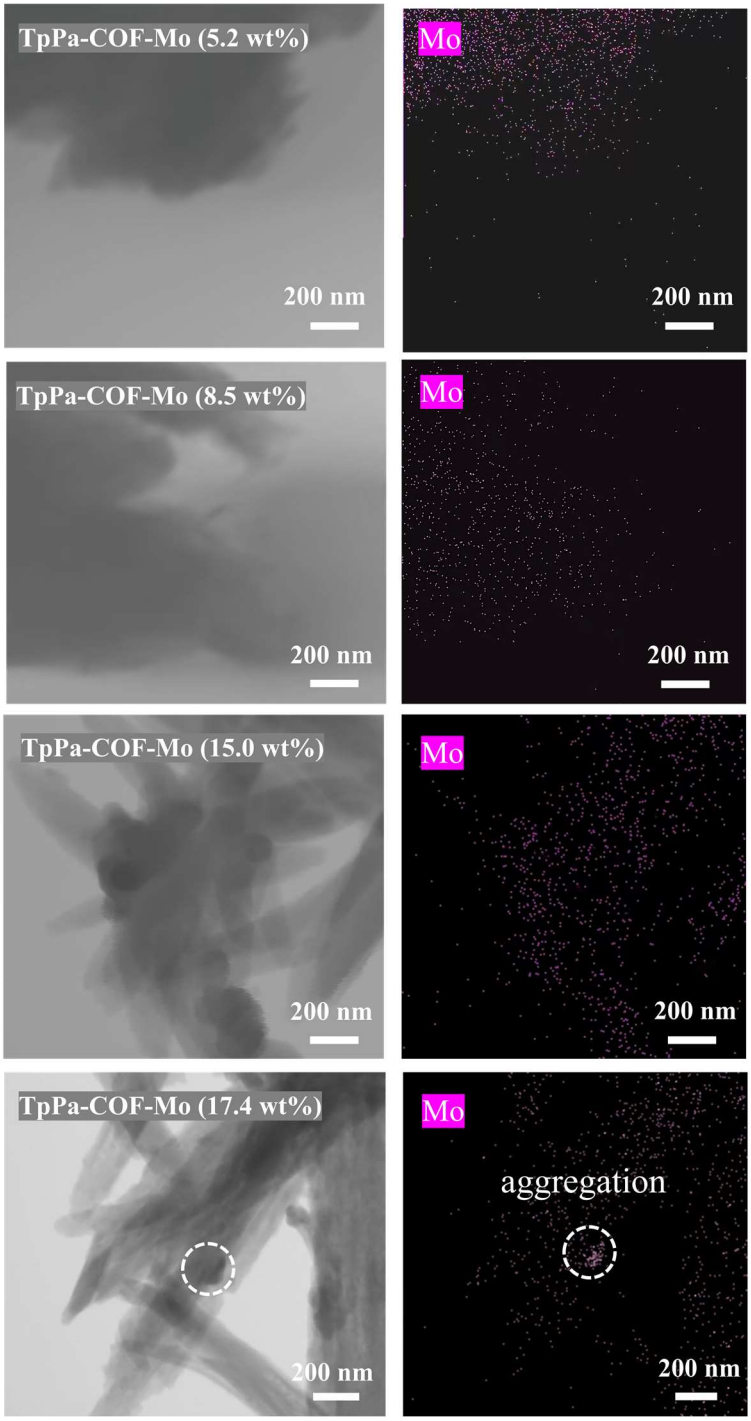

Figure S29. TEM images and EDX elemental mapping of Mo in TpPa-COF-Mo samples with varying Mo loadings.

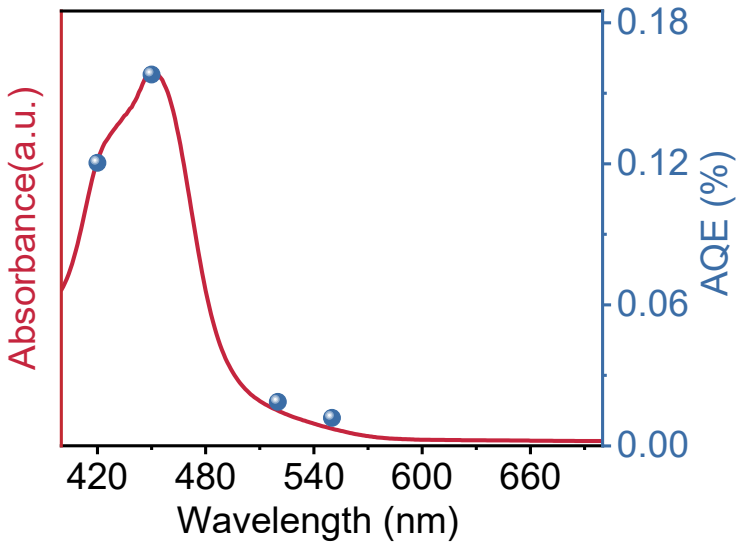

Figure S30. AQE of C_2H_6 production catalyzed by TpPa-COF-Mo at different wavelengths and the related visible spectrum.

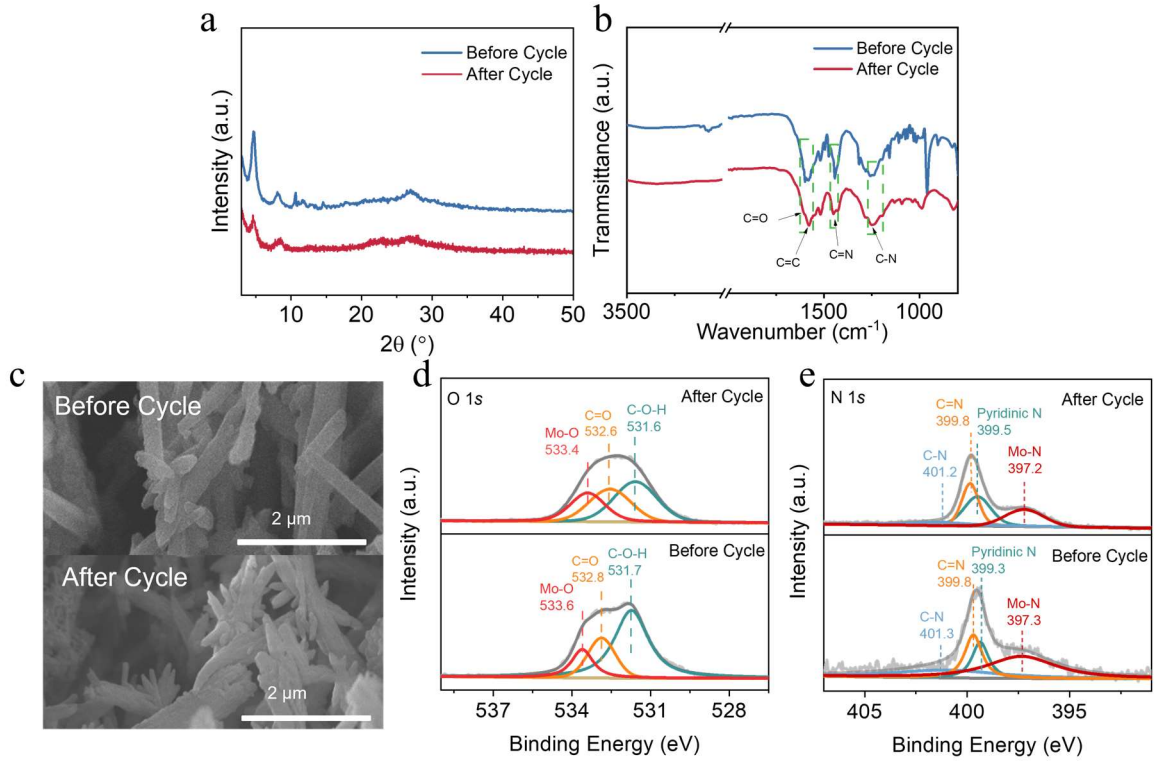

Figure S31. Chemical stability of TpPa-COF-Mo before and after 4 cycles of CO_2 photoreduction process. (a) XRD patterns. (b) FTIR spectra. (c) SEM images.(d-e) XPS spectra.

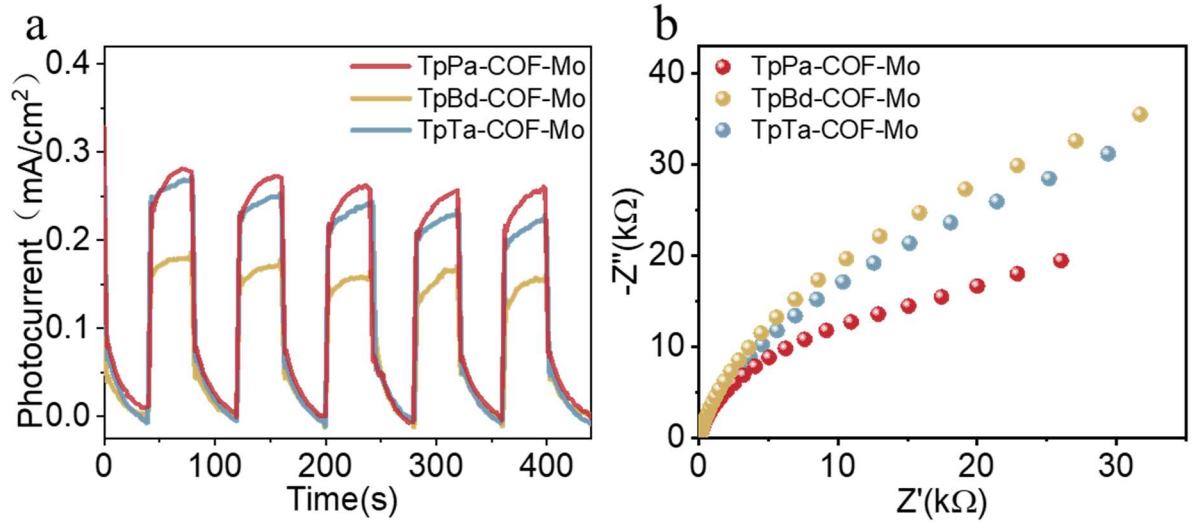

Figure S32. (a) Transient photocurrent spectra under 300 W xenon lamp (≥420 nm) irradiation for Tp-COFs-Mo and (b) Nyquist plots of Tp-COFs-Mo obtained from electrochemical impedance spectroscopy measurements.

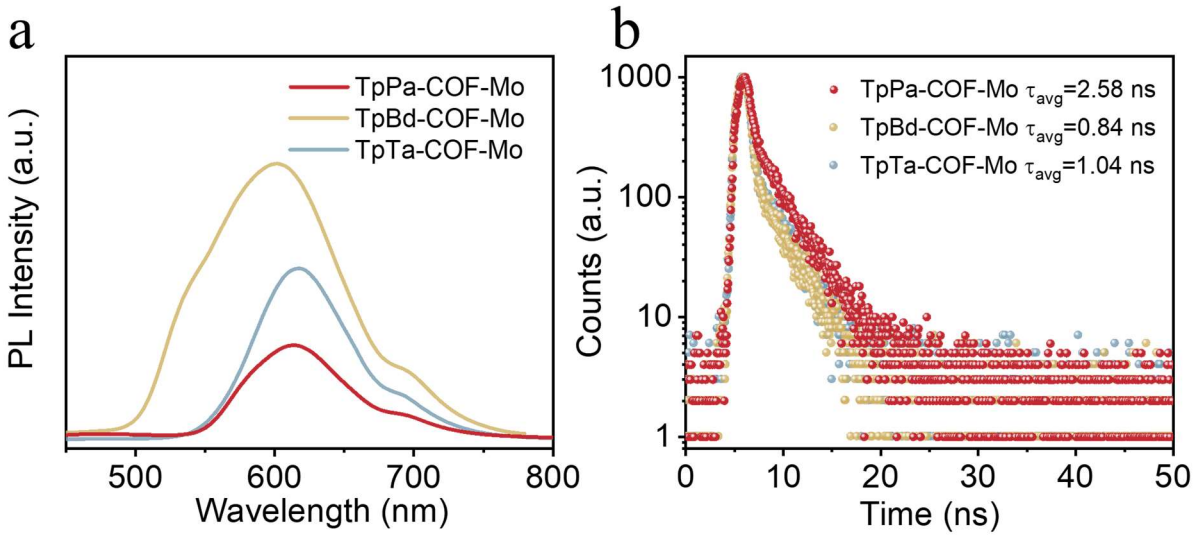

Figure S33. Steady-state PL spectra and PL decay spectra of Tp-COFs-Mo.

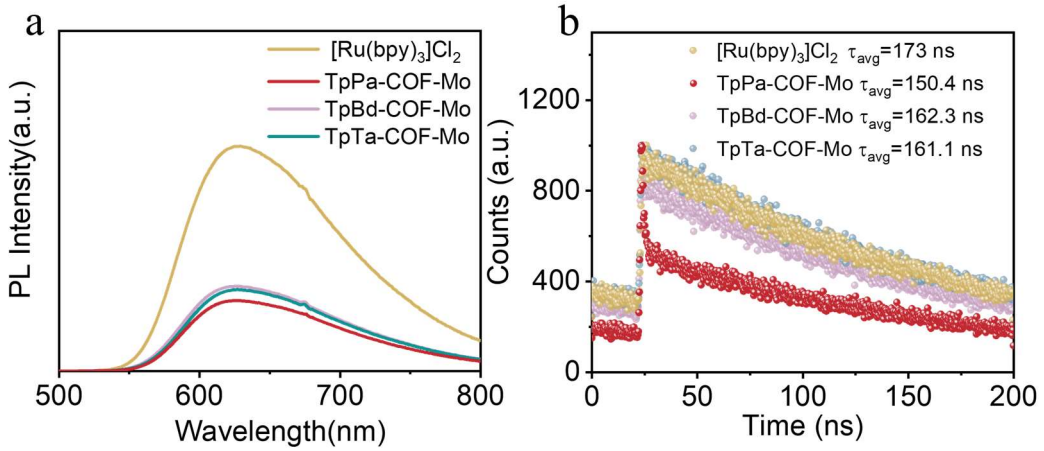

Figure S34. (a) Steady-state PL spectra and (b) PL decay spectra of Tp-COFs-Mo in photoreaction system including $[Ru(bpy)_3]Cl_2$ and Tp-COFs-Mo

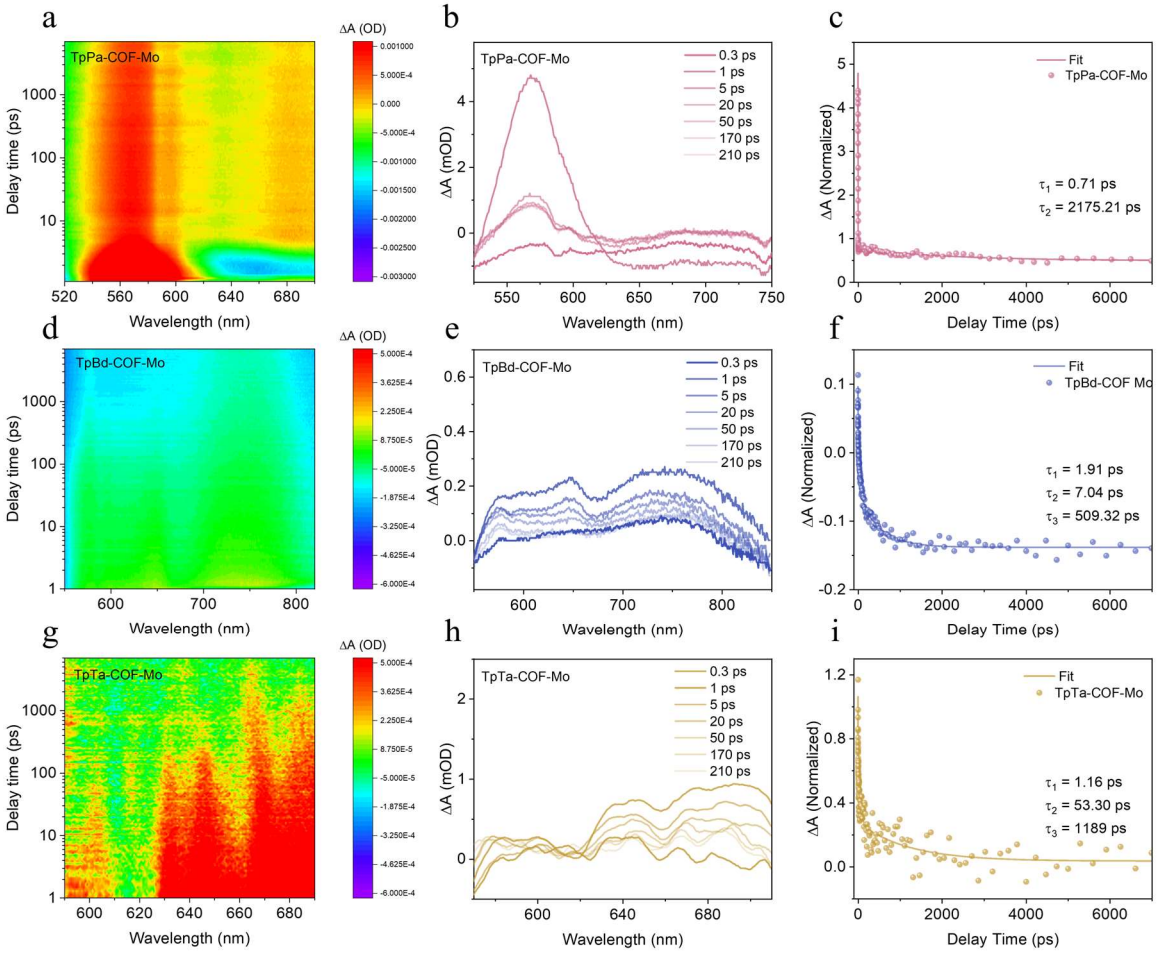

Figure S35. Pseudocolor fs-TA plots of (a) TpPa-COF-Mo, (d) TpBd-COF-Mo and (g) TpTa-COF-Mo, Transient absorption spectra recorded at the indicated delay times of (b) TpPa-COF-Mo, (e) TpBd-COF-Mo and (h) TpPa-COF-Mo measured at an excitation of 405 nm. Normalized transient absorption kinetic traces of (c) TpPa-COF-Mo, (f) TpBd-COF-Mo, and (i) TpTa-COF-Mo monitored at 570 nm, 742 nm, and 680 nm, respectively.

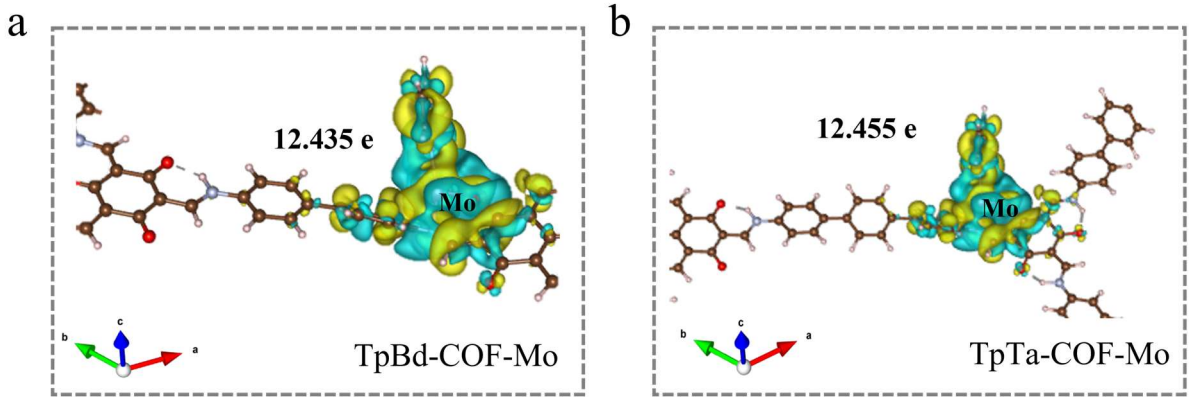

Figure S36. Isosurfaces (level 0.0002 eV·Å^{-3}) of charge density differences of (a) TpBd-COF-Mo, and (b) TpTa-COF-Mo.

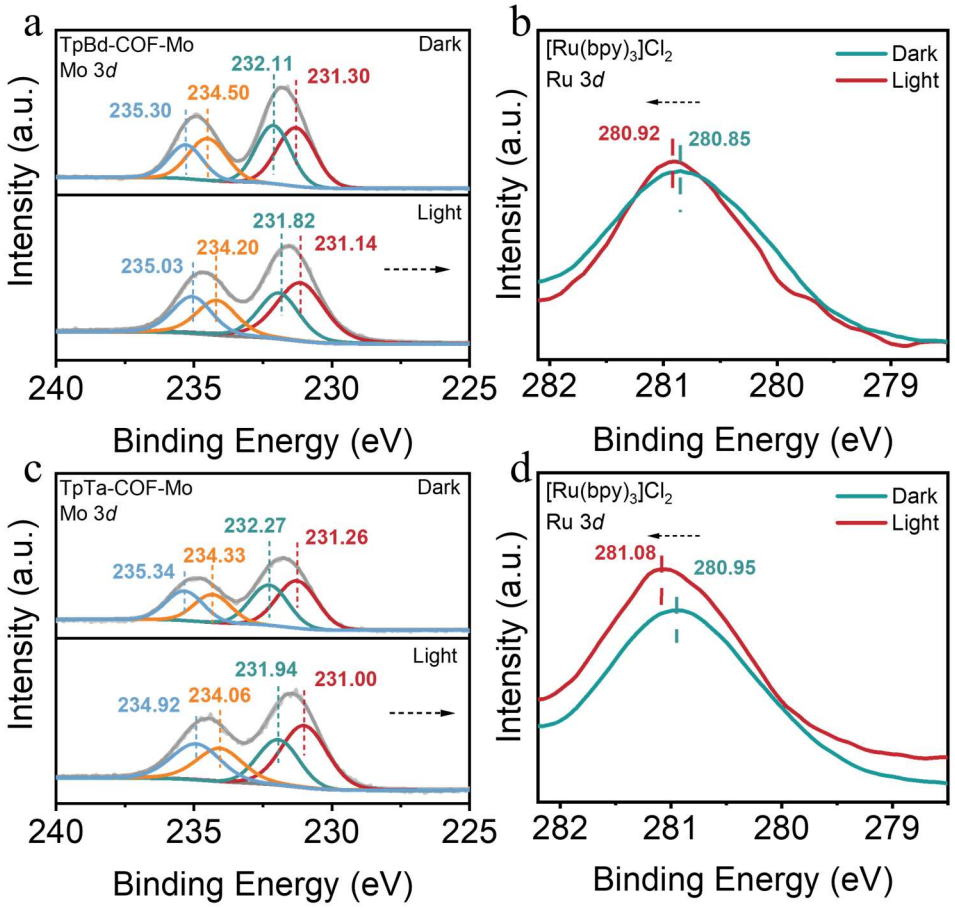

Figure S37. Quasi-in situ XPS spectra of (a) Mo 3*d* and (b)Ru 3*d* for $[Ru(bpy)_3]Cl_2$ and TpBd-COF-Mo, (c) Mo 3*d* and (d) Ru 3*d* for $[Ru(bpy)_3]Cl_2$ and TpTa-COF-Mo under light and in the dark.

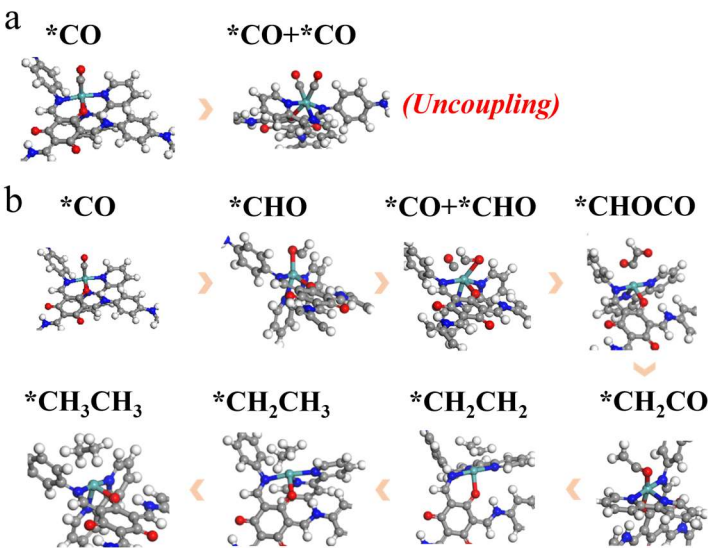

Figure S38. The intermediates of CO_2RR to C_2H_6 over TpPa-COF-Mo. (a) *CO+*CO coupling pathway (Cannot be directly coupled to generate *OCCO). (b) *CO+*CHO coupling pathway.

3. Supplemental Tables S1-5

Table S1. Molybdenum content in TpPa-COF-Mo, TpBd-COF-Mo and TpTa-COF-Mo determined by ICP-MS

Sample	Metal	ICP-Content (wt.%)
TpPa-COF-Mo	Mo	15.0
TpBd-COF-Mo	Mo	15.7
TpTa-COF-Mo	Mo	15.3

Table S2. Structural parameters of the TpPa-COF-Mo, TpBd-COF-Mo and TpTa-COF-Mo obtained from EXAFS fitting

Condition	**Path**	***CN***	***R* (Å)**	**σ^2 (10^{-3}Å^2)**	**ΔE_0 (eV)**	R factor
Mo foil	Mo-Mo	8	2.71	4.2	9.1	0.01
	Mo-Mo	6	3.11	4.4	9.1	
TpPa-COF-Mo	Mo-N	2.1	1.94	3.0	8.14	0.021
	Mo-N	1.2	2.08	3.0	8.14	
	Mo-O	0.9	1.99	3.0	8.14	
TpBd-COF-Mo	Mo-N	2.3	2.01	3.0	7.93	0.011
	Mo-N	1.1	2.07	3.0	7.93	
	Mo-O	1.1	1.99	3.0	7.93	
TpTa-COF-Mo	Mo-N	1.9	2.01	3.0	7.34	0.024
	Mo-N	1.0	2.09	3.0	7.34	
	Mo-O	1.2	1.98	3.0	7.34	

CN is the coordination number for the absorber-backscatter pair, R is the average absorber-backscatter distance, σ^2 is the Debye-Waller factor, and ΔE_0 is the inner potential correction. S_0^2 was fixed to 0.80 as determined from Mo foil fitting. The accuracy of the above parameters is estimated as CN, ±20%; R, ±1%; σ^2, ± 20%; ΔE_0, ±20%.

Table S3. Performance comparison of COF-, POP-, and MOF-based photocatalysts for CO_2RR to C_2H_6 under broadly comparable conditions

Photocatalyst	Catalyst mass	Catalytic condition	Light	Production Rate of C_2H_6 ($\mu mol\ g^{-1}\ h^{-1}$)	C_2H_6 electron selectivity (%)	TOF	Reference
TpPa-COF-Mo	2 mg	$[Ru(bpy)_3]Cl_2 \cdot 6H_2O$ TEOA, MeCN, H_2O	300 W Xe lamp (420-780 nm) 300 $mWcm^{-2}$	**262.6**	**91.8**	**0.168**	This work
TpBd-COF-Mo				82.6	70.1	0.051	
TpTa-COF-Mo				143.7	79.1	0.091	
CuPor-POP-Mo	5 mg	$[Ru(bpy)_3]Cl_2 \cdot 6H_2O$ TEOA, MeCN, H_2O	300 W Xe lamp (420-780 nm) 300 $mWcm^{-2}$	472.5	97.5	0.533	[3]
MoS_2@COF	1mg	$[Ru(bpy)_3]Cl_2 \cdot 6H_2O$ TEOA, MeCN, H_2O	300 W Xe lamp (420-780 nm) 209 $mWcm^{-2}$	56.2	83.8	-	[10]
TiO_2(x)@UiO-67 MOFs	50 mg	TEOA, MeCN, H_2O	300 W Xe lamp UV cut-off filter ($\lambda > 420$ nm)	79.3	100	-	[11]
Cu-CuTCPP/g-C_3N_4	5 mg	TEA, H_2O	300 W Xe lamp (360-800 nm) 150 $mWcm^{-2}$	18.5	68.8	-	[12]
Cu@Py-BTDA-COF	10 mg	TEOA, H_2O	300 W Xe lamp 400 $mWcm^{-2}$	93.2	88.4	0.128	[13]
$CABB_{20}$/UiO-66	20 mg	ethyl acetate, TEA, H_2O	300 W Xe lamp 420 nm cut-off filter 230 $mWcm^{-2}$	1.3	8.8	-	[14]
Cu(X)@NH_2-UiO-68 MOFs	50 mg	TEOA, MeCN, H_2O	300 W Xe lamp UV cut-off filter ($\lambda > 420$ nm)	51.3	98.8	0.0659	[15]
CuCo/Ti-MOF-Py-Ru	20 mg	TEOA, MeCN, H_2O	300 W Xe lamp 400 nm cut-off filter	0.55	-	-	[16]

Table S4. Apparent quantum efficiency (AQE) of TpPa-COF-Mo at different wavelengths

Wavelengths (nm)	Intensity (mW cm^{-2})	AQE (%)
420	16.83	0.13
450	17.50	0.15
520	20.52	0.07
550	23.80	0.04

Table R5. AQE comparison of COF-based photocatalysts for CO_2RR to C_2H_6

Photocatalyst	Production rate C_2H_6 ($\mu mol\ g^{-1}\ h^{-1}$)	C_2H_6 electron selectivity (%)	AQE	Reference
TpPa-COF-Mo	262.6	91.8	0.15%	This work
MoS_2@COF	56.2	83.8	0.03%	*Appl. Catal. B: Environ.* 2023, 325, 122393
Cu@Py-BTDA-COF	93.2	88.4	None	*Appl. Catal. B: Environ.* 2025, 377, 125499
CuPor-POP-Mo	472.5	97.5	0.55%	*Chem. Sci.* 2025, 15, 15166-15176

4. Supplemental References

[1] Q. Zhang, S. Gao, Y. Guo, H. Wang, J. Wei, X. Su, H. Zhang, Z. Liu, J. Wang, *Nat. Commun.* **2023**, *14*, 1147.

[2] X. Yang, L. Ren, Z. Chen, H. Li, Y. Yuan, *Adv. Mater.* **2025,** *37*, 2412299.

[3] Q. Zhang, S. Gao, X. Zhao, H. Wang, Y. Guo, Z. Liu, J. Wang, *Chem. Sci.* **2025**, *15*, 15166-15176.

[4] N. Huang, H. He, S. Liu, H. Zhu, Y. Li, J. Xu, J. Huang, X. Wang, P. Liao, X. Chen, *J.Am.Chem.Soc.* **2021**, *143*, 17424-17430.

[5] G. Wang, Y. Wu, Z. Li, Z. Lou, Q. Chen, Y. Li, D. Wang, J. Mao, *Angew. Chem. Int. Ed*. **2023**, *62*, e202218460.

[6] G. Kresse, J. Furthmüller, *Comput. Mater. Sci.* **1996**, *6*, 15-50.

[7] G. Kresse, D. Joubert, *Phys. Rev. B*. **1999**, *59*, 1758-1775.

[8] J. P. Perdew, K. Burke, M. Ernzerhof, *Phys. Rev. Lett*. **1996**, *77*, 3865-3868.

[9] S. Grimme, J. Antony, S. Ehrlich, H. Krieg, *J. Chem. Phys*. **2010**, *132*, 154104.

[10] X. Yang, X. Lan, Y. Zhang, H. Li, G. Bai, *Appl. Catal. B Environ.* **2023**, *325*, 122393.

[11] M. J. Saadh, M. A. Mustafa, F. M. A. Altalbawy, S. Ballal, G. V. S. Prasad, M. J. Al-Saray, J. K. Abbas, M. A. Al-Maliky, S. K. Mohammed, M. M. Alam, A. Elawady, *J. Mol. Struct.* **2025**, *1325*, 140830.

[12] S. Xie, Y. Li, B. Sheng, W. Zhang, W. Wang, C. Chen, J. Li, H. Sheng, J. Zhao, *Appl. Catal. B Environ.* **2022**, *310*, 121320.

[13] X. Chen, C. Liu, T. Yang, X. Jiang, Y. Yang, J. Su, J. Yi, Y. Dong, *Appl. Catal. B Environ.* **2025**, *377*, 125499.

[14] W. Xiong, W. Ouyang, M. Li, H. Song, C. Zhao, M. Hu, S. Bai, Y. Liu, Y. Wu, Y. Zhang, Y. Liu, A. Pan, *Appl. Surf. Sci*. **2024**, *644*, 158807.

[15] Z. Al-Khafaji, F. M. A. Altalbawy, N. Y. Jamil, A. S. Sahib, A. Hashem, Z. A. Hamodi, S. H. Hamo, Z. S. Abdulali, M. Alwan, M. Jawad, H. Mushtaq, K. Muzammil, *Mol. Catal*. **2025**, 587, 115494.

[16] L. Ye, L. Su, W. Cen, D. Sun, *Nanoscale*. **2025**, 17, 11345-11352.